Interaction of sea ice floe size, ocean eddies, and sea ice melting

Interaction of sea ice floe size, ocean eddies and sea ice melting

Christopher Horvat,[1] Eli Tziperman,[1] Jean-Michel Campin,[2]

Key Points.

- Sea-ice melting rates are sensitive to floe sizes in the range of 1-50 km, larger floes than previously assumed.
- Ocean eddies that develop due to density gradients at floe edges lead to enhanced melting of floes at their boundaries.
- Eddies therefore effectively melt floes laterally, with smaller floes melting more rapidly per unit of sea-ice area.

The effect of the horizontal size of sea-ice floes on sea-ice melting is commonly formulated using the ratio between side and basal floe area. This lead to the conclusion that floe size was not important for sea-ice evolution when floes exceed about 30 meters. This paper considers a mutual interaction between floe size, ocean circulation, and melting. We find that lateral density gradients form at the boundaries of floes, and drive ocean-mixed-layer instability and energetic eddies that spread from the ice edge. The resulting circulation mixes heat horizontally, melting floes near their edges. Idealized ocean model experiments show the sea ice response is sensitive to floe size in the range of 1-50 km, considerably larger than previously assumed important, as smaller floes melt more rapidly per unit ice area. It is proposed that the role of eddies and floe size distribution should be incorporated into current climate models.

1. Introduction

Sea ice is a major part of Earth's climate system, mediating the exchange of heat and fresh water via its albedo and insulating properties, and moderating momentum exchange between the high-latitude oceans and atmosphere via its mechanical behavior and internal stresses. It is a potential cause of past abrupt climate changes [*Gildor and Tziperman*, 2003] and has been changing rapidly in recent years [*Stroeve et al.*, 2012]. The sea-ice cover itself is a mosaic of individual floes with a wide range of sizes and shapes, and is typically described statistically, using the ice thickness distribution [ITD, *Thorndike et al.*, 1975], or floe size distribution [FSD, *Rothrock and Thorndike*, 1984]. Previous studies have shown that sea-ice edges may lead to the development of eddy motions in the ocean. Openings (leads) that form in the winter-time sea ice re-freeze, rejecting cold, dense brine, which sinks, creating a sharp density front in the upper ocean that leads to ageostrophic overturning and ocean eddies [*Smith*, 2002; *Matsumura and Hasumi*, 2008].

Sea-ice models used in current global climate models (GCMs) simulate the ITD, but not the FSD. The distribution of floe sizes may, however, be an important climate variable, as the size of floes influences the response of the sea-ice cover to external stresses [*Feltham*, 2005; *Herman*, 2013], the response of sea ice to external heating events [*Steele*, 1992; *Asplin et al.*, 2012], and turbulent exchange in both the oceanic and atmospheric boundary layers [*Birnbaum and Lüpkes*, 2002].

In current GCMs, the magnitude of a net warming heat flux exchanged between the ocean and sea ice is proportional to the total surface area of the sea-ice cover in a grid cell. This heat flux can lead to melting at the lateral (floe edge) and basal ice surfaces. The partitioning of a net heat flux parameterized in this way between lateral and basal melting is based on the ratio between the two areas, which in some GCMs may be a function of a specified floe size parameter that does not change. Floe diameters are often several kilometers or more, but floe thicknesses are seldom more than 10 m, therefore the ratio of lateral surface area to basal surface area is small, therefore melting at the lateral edges of floes may not play a major role in the global sea-ice volume budget. Indeed, the contribution of lateral melting parameterized in this way to sea-ice volume changes is commonly assumed to be sensitive to floe size only when the mean floe diameter is O(30) meters or smaller [*Steele*, 1992]. Such small floes do not comprise a major fraction of the ice-covered oceans. Modern GCMs therefore do not attempt to evolve floe size, and either include a fixed mean floe size parameter [*Hunke and Lipscomb*, 2008], taken to be at least 300 meters, implicitly assuming the effect of floe size on melting is negligible, or ignore floe size altogether and compute lateral melting as an indirect consequence of vertical melting [*Hibler*, 1979; *Notz et al.*, 2013].

In spite of this common assumption, the size of floes is expected to affect sea ice melt rates. Consider, for example, a pulse of shortwave heating at the ocean surface due to a short term clearing of low clouds in the Arctic in late spring or summer, after the breakup of the winter pack ice. Ice melting creates a cold, freshwater lens underneath floes. Regions not covered by sea ice are heated by the atmosphere and do not change their salinity, thereby becoming relatively salty and warm compared to the ice-covered regions. At low temperature, the influence of temperature on density is negligible [*Timmermans and Jayne*, 2016], so that the salinity gradient leads to a strong density gradient across the floe edge, which may be baroclinically unstable. This gradient is then erased by mixing due to ocean eddies which carry heat from the warmer ice-free ocean underneath the edges of floes. The resulting warming of water underneath the floe edges leads to further ice melting, while regions of the upper-ocean near the interior of larger floes, away from the effect of the eddies, remain cold. Ice melting is thus enhanced at the margins of floes. The efficiency of the mixing is a function of the length scales of the eddies and of the floes, and for the same initial sea-ice volume, regions of sea

[1]Department of Earth and Planetary Sciences and School of Engineering and Applied Sciences, Harvard University, Cambridge, MA, USA

[2]Earth, Atmospheric and Planetary Sciences Department, Massachusetts Institute of Technology, Cambridge, MA, USA

0094-8276/16/$5.00

ice with smaller floe sizes and more sea-ice perimeter may melt faster. This is the idea tested in this paper.

As of yet, no studies gauged the relationship between floe size, ocean circulation and eddies, and sea-ice melting, yet the above scenario by which ocean eddies may lead to enhanced melting at floe edges suggests that the size of floes may influence the evolution of sea ice in melting conditions. We test this hypothesis by performing idealized high-resolution ocean model experiments with "floes" of prescribed size, studying the development of the ocean circulation and evolution sea-ice area as a function of floe size. The main novel results are: (1) the interaction of air-sea fluxes and the melting of sea-ice floes leads to density fronts, a floe-edge jet and overturning circulation, baroclinic instability, and an energetic eddy field developing near the floe edges. (2) The floe-edge circulation and eddies exchange heat between open-water areas and ice-covered regions, enhancing vertical sea-ice melting rates along floe perimeters, and effectively reducing floe area. (3) As a result, the rate of sea ice volume loss is sensitive to floe sizes in the range 1 km-50 km, much larger than the 30 m range considered previously. For different floe size distributions, this may be manifested as a several-month difference in the time it takes an ocean area equivalent in size to a GCM grid cell to become ice-free during the melting season.

The paper proceeds as follows: we describe the model experiments used to examine the interaction between the FSTD, ocean eddies, and sea ice melting in section 2. We analyze the model response in section 3. We conclude in section 4.

2. Model description

We use the MIT general circulation model [MITgcm, *Marshall and Hill*, 1997; *Losch et al.*, 2010], with sea ice simulated using the thermodynamic sea ice package of the MITgcm, based on the two-layer thermodynamic model of *Winton* [2000], simulating a single thickness at each grid point. Vertical mixing is realized using the K-profile parameterization mixing scheme [*Large et al.*, 1994]. In the simulations described below, surface heating and ice melting stratify the the surface ocean, and no convection is therefore realized. In addition, the background vertical mixing is very small and on the time scales of interest here cannot affect the stratification and instability growth rate (see Sec. 3, Eq. 2). Horizontal eddy viscosity is represented by the Smagorinsky scheme. No horizontal diffusion is used in order for the circulation that develops to accomplish any horizontal mixing. The fully nonlinear equation of state of *McDougall et al.* [2003] is used. The *Deremble et al.* [2013] atmospheric boundary layer model was adapted for use with sea ice in order to simulate the turbulent fluxes between the ocean, sea ice, and atmosphere. The use of an atmospheric boundary layer model is important because it evolves the atmospheric temperature in response to the presence or absence of sea ice, which in turn affects the computed heat fluxes over sea ice and open water. A full description of the model configuration and list of model parameters used in these runs are provided as supporting information (Text S1, Table S1).

The ocean domain is configured as a hydrostatic reentrant zonal channel on an f-plane, 75 km wide in both directions, with walls on the northern and southern boundaries. There are 300 grid points in each horizontal direction, and 50 in the vertical direction. The horizontal grid spacing is 250 m. The vertical grid spacing is 2.5 m over the top 75 m, increasing by 20% at each subsequent grid point to a total depth of 1 km, following *Fox-Kemper et al.* [2008].

The ocean is initialized using the July climatological temperature and salinity profile from the Fram Strait ($80^\circ N$,0° E, Fig. 1e) [*Carton and Giese*, 2008], with the top 50 meters of the water column homogenized to create a mixed layer. This depth is similar to observations of Arctic mixed layer depths [*Peralta-Ferriz and Woodgate*, 2015]. We considered the degree to which the near-surface stratification influences model results by performing a sensitivity analysis to mixed layer depth (Supporting Information, Text S3), either by extending the stratification to the surface or imposing mixed layer depths of 25 meters or 100 meters. The results below, which indicate that the rate of ice melting depends on the size of floes, are not sensitive to this choice.

To allow instabilities to develop, the top 50 m of the temperature field is seeded with small amplitude white noise uniformly distributed between $\pm 0.025^\circ$C. The atmospheric temperature is initialized at $T_a = -10^\circ$C and the atmospheric boundary layer height is set to 1 km. A horizontally and temporally uniform (no diurnal cycle) shortwave forcing of 210 W/m^2 and longwave forcing of 220 W/m^2 is applied at the ocean surface.

To simulate floes, each grid point is initialized with an ice concentration of either 0 (open water) or 1 (ice). "Floes" are formed by combining ice-covered grid points into regions with one of six configurations of sea ice, with either 1 floe, 4, 16, 64, $16 \times 16 = 256$ and $36 \times 36 = 1296$ floes (four of the floe configurations are shown in Fig. 1(a-d)), with a domain average concentration of 49.92%. The floes are spaced uniformly over the ocean surface, with an intra-floe spacing that ranges from 50 km (in the case of 1 floe) to 1 km (in the case of 1296 floes). . A seventh run has a uniform ice concentration of 49.92% specified at every model grid point.

Sea ice points are initialized with an internal temperature of -5° C, and an initial thickness of 1 m. Each model run therefore has the same initial domain-averaged sea-ice volume, area fraction, and albedo. We disable the sea ice momentum equations, and therefore the advection of sea ice, in order to isolate the thermodynamic response of the sea ice cover and use a free-slip boundary condition for the ocean at the interface with sea ice. The MITgcm sea-ice package used does not represent a submerged component of the sea-ice cover. A heat flux between the ocean and sea ice is still partitioned into two components: one that leads to changes in ice concentration and one that leads to changes in ice thickness. The default partition uses a power-law relationship of ice concentration and thickness, but the model results are not sensitive to changes in this partitioning (Supporting Information, Text S2-S3).

3. Floe size effects on the melting of sea ice

Fig. 2 shows the ocean circulation and density structure near a single floe in the one floe experiment (Fig. 1a), at day 5, before eddies develop, and at day 50, when they are more fully developed. The balance of heat fluxes over open water include imposed fluxes of shortwave heating (210 W/m^2) long-wave heating (220 W/m^2) representative of spring-summer conditions in the Arctic [*Kanamitsu et al.*, 2002]. Model computed sensible cooling (39 W/m^2) and upward long-wave cooling (300 W/m^2), leads to a net ocean warming with an initial magnitude of 91 W/m^2, ranging from 90-94 W/m^2 over the course of the simulation. There is no evaporation, sublimation, or precipitation and therefore no latent heat flux exchanged between the ocean-ice and atmosphere. Fig. 2(a-c) plots profiles of the mean ocean density (Fig. 2a), temperature (Fig. 2b), and salinity (Fig. 2c) at day 5 (dashed lines) and 50 (solid lines). "Ice-covered" regions (red lines in Fig. 2a-c) are defined as those with at

least 90% ice concentration. Open-water regions (blue lines in Fig. 2a-c) are all other regions.

Heating of the sea ice from below due to surface ocean temperatures being above freezing leads to a shallow lens of relatively fresh ($\Delta S \approx 0.8$ ppt) and cold ($\Delta T \approx$ -1.5° C) water in the ice-covered region (Fig. 2b-c, red lines) relative to the open-water region, where shortwave heating increases the ocean temperature. The density gradient between under-ice and open-water regions (Fig. 2a,d Fig. 2f,g) is dominated by this gradient in salinity, and leads to a geostrophically-balanced surface jet that moves counter-clockwise along the floe edge (Fig. 2h), with a maximum magnitude of 5 cm/s, and mean magnitude of 2.5 cm/s. A deeper counter current of a similar magnitude flows clockwise at the mixed-layer base. The floe-edge current has an associated ageostrophic overturning circulation, with a cross-front velocity at the ice edge, from the open water to underneath the ice (Fig. 2h, dashed contours), due to a balance between vertical dissipation of the along-floe current and Coriolis acceleration. This cross-edge horizontal velocity is part of a narrow overturning circulation, with downwelling at the floe edge and upwelling just outside the floe (Fig. 2f), replacing the cold, fresh under-ice water with saltier, warmer water from the ice-free region.

The strong, shallow lateral density gradients at the floe edge are baroclinically unstable, with instabilities appearing along the front within several days and growing in time (Fig. 2d,e). Instability is confined to the mixed layer, where the Richardson number, defined as (Fig. 2a,h),

$$Ri \equiv \frac{N^2}{|\frac{\partial u}{\partial z}|^2} \approx \frac{Hg}{\rho_0}\frac{\rho(0)-\rho(-H)}{|u(0)-u(H)|^2} \approx 0.5 \cdot \frac{0.4}{0.025^2} \approx 300, \quad (1)$$

is high. The spatial scale of the unstable motions along a horizontal density gradient may be estimated as the first baroclinic deformation radius [*Tandon and Garrett*, 1994],

$$L_d = \frac{NH}{\pi f} = \frac{g}{\pi \rho_0}\left|\frac{\partial \rho}{\partial x}\right|\frac{H}{f^2} \approx \frac{9.81}{1000}\frac{0.3}{3000}\frac{50}{10^{-8}}\,\mathrm{m} \approx 5\mathrm{km}.$$

These instabilities are ageostrophic, with local Rossby number, defined as $Ro \equiv (\frac{\partial v}{\partial x} - \frac{\partial u}{\partial x})/f$, approaching 0.5 (Fig. 4b,d). The maximum growth rate, σ_{max}, of ageostrophic baroclinic instability [*Stone*, 1966] is,

$$\sigma_{max}(Ri) \approx 0.3\sqrt{\frac{f^2}{1+Ri_b}} = \frac{1}{6.6 \text{ days}}. \quad (2)$$

Eddy mixing slumps tilted isopycnals, exchanging buoyancy between the open water (warm, salty) and ice-covered regions (cold, fresh) at the floe boundaries, delivering warmer waters to the ice base in the regions in which eddies are active (Fig. 2e), and enhancing melting there. This melting can also contribute to restratification under the ice, acting to weaken the eddies. Videos of the surface density field and sea ice volume, which demonstrate the development of eddies and subsequent sea-ice melting, are included as supporting information (Movies S1-S2).

The time evolution of the sea-ice volume is seen in Fig. 3a for each model run. Experiments with a larger number of (smaller) floes, yet with the same total initial ice area, show faster melting. This is an important result, as the physics that leads to this difference is not resolved in current climate models. The eddies lead to an enhanced delivery of heat from the open ocean to the ice covered areas at the floe perimeter. The ice cover therefore melts more rapidly when the total floe perimeter length is larger (that is, when the number of floes is larger). For satellite observations of the polar regions, a region is considered "ice-free" for the purposes of calculating sea ice extent when the mean ice concentration drops below 15%. Using this as rule of thumb, we define an "ice-free" threshold, when the mean ice volume is decreased to below 0.15 $\mathrm{m}^3/\mathrm{m}^2$ (dashed line, Fig. 3a). It takes 70 days to reduce the sea ice volume to this level in the 1296 floe case, and 69 additional days for the single-floe case (it takes 59 days in the case of a uniform ice cover).

Baroclinic instability converts available potential energy (APE) into eddy kinetic energy (KE). We calculate the APE as the difference between total potential energy ($\rho g h$) and the minimum possible potential energy that the fluid can attain, by sorting the density field following *Huang* [2005], and the results are shown in Fig. 3c. Over the first 50-60 days, the difference in surface forcing between the ice-covered and open water regions leads to increasing floe-edge density gradients and APE, which are later eliminated as the eddies spread and convert APE to KE (Fig. 3b), as is typical of upper-ocean baroclinic instability [*McWilliams*, 1985; *Tandon and Garrett*, 1994; *Boccaletti et al.*, 2007]. As larger floes are insulated at their interior from the eddies, the density gradient between under-ice and open-water regions can grow longer before being reduced by eddies, and the corresponding runs have higher maxima in APE and KE. As the eddies take longer to consume the APE for larger floes, these maxima also occur later. As APE is converted to KE, in all experiments, KE continues to increase after APE begins to decrease. Later, the KE source from this conversion is dominated by other effects, including dissipation.

The spread of eddies and corresponding mixing of heat toward the interior of floes, are shown in Fig. 4. Hovmöller diagrams of the top 10 meter temperature averaged over the meridional extent of a floe are shown for two experiments: the 16-floe experiment (Fig. 4a, corresponding to the region outlined in black in Fig. 1b), and the single-floe experiment (Fig. 4c, corresponding to the region outlined in black in Fig. 1a). Mixing at the ice edge spreads heat into the interior of floes at a rate of roughly 1 km per 3 days, which is more effective at reaching the interior of smaller floes than large ones. Given that no explicit horizontal diffusion is used in these experiments, all of the horizontal mixing is accomplished by the combination of eddies and the advective floe-edge circulation. From Fig. 4, one can estimate an effective eddy diffusivity. Mixing at the ice edge spreads heat into the interior of floes at a rate of roughly 1 km per 3 days, which is more effective at reaching the interior of smaller floes than large ones. The eddies therefore permeate a distance of $L = 25$ km over a time-scale of $\Delta t = 72.5$ days, giving an eddy diffusivity of $\kappa_h \approx L^2/\Delta t = 100$ m^2/s, in line with calculations of eddy diffusivity found in simulations of sub-mesoscale frontal systems [*Boccaletti et al.*, 2007]. Figs. 4(b,d) show the Rossby number at day 24 of the simulation, either around one of the 16 floes (the red shaded region in Fig. 1b), or at the floe-edge in the single floe experiment (the red shaded region in Fig. 1a), with an equal total area shown in both figures. The eddy mixing is capable of nearly penetrating the interior of the smaller floe (Fig. 4b), but is confined at the ice edge for the larger floe (Fig. 4d).

A consequence of the eddy transport of heat toward the floe interior is that small floes melt faster, shown by the white contours in Fig. 4(a,c). This is our main result, and is consistent with the scenario depicted in the introduction. It explains that larger floes will take longer to melt, given an ocean area covered with the same sea-ice fraction but with different floe size. Furthermore, the melting due to the eddy heat transport occurs mostly near floe edges, which means that this mechanism effectively changes floe area rather than

thickness. The relationship between sea-ice concentration and volume therefore depends on the floe size for a large range of floe sizes, controlled by the interplay of floe size and the circulation or eddies generated at floe boundaries. These experiments therefore demonstrate a complex interaction between ocean circulation, eddies and floe size during sea-ice melting, and the need to represent these processes in climate models, either directly or via a parameterization.

4. Conclusions

We showed here that surface ocean density gradients generated at the edge of sea-ice floes due to sea-ice melting and air-sea heat fluxes lead to a floe-edge circulation, mixed-layer instability, and eddies, with instability growth timescales of less than 10 days and eddy length scales of less than 10 km. We further showed that the floe-edge circulation and eddies play a major role in mixing heat from open water areas toward the area under floes, leading to enhanced melting there. Larger floes are more insulated from these processes at the floe edge, and melt slower. This effect leads to a strong dependence of the time evolution of sea-ice area and volume on the size distribution of floes.

This strong relationship between sea-ice melt rates and floe size depends upon sub-grid scale processes not included in current GCMs and sea ice models. Current models are commonly based on the hypothesis that the influence of floe sizes on lateral melting is only effective for floes smaller than about 30 m, much smaller than indicated by our results. We find the eddy heat transport at floe edges enhances the rate of basal melting near the perimeter of floes, effectively acting as an agent of lateral melting. This mechanism is effective for floes with horizontal scales of 1-50 km, and is shown here to play a leading order role in the melting of large floes. This coupling between eddies and sea ice melting leads to different melt rates for different floe sizes, and a difference of several months in the time it takes an ocean domain to become ice free. These effects may be particularly important in seasonal ice zones, which break up and then melt over the course of each year, the experimental setup considered above. As most of the Antarctic is already seasonal, and the Arctic is rapidly progressing to being entirely seasonal [*Overpeck et al.*, 2005; *Aksenov et al.*, 2016], the importance of this effect could potentially grow.

The model experiments used here are by necessity highly idealized, with a uniform mixed layer, starting from a rest ocean state, and ignoring ice advection. These simplifications are used to isolate this particular feedback between ocean eddies, floe size and melting. Other processes, like advection by wind and ocean currents and frictional mixing between the ocean and ice due to ice roughness have been ignored in order to isolate the influence of this ice-edge mechanism. Our choice to start with a resting ocean makes sense when considering the melting of a region of sea ice in relatively calm conditions. The density gradients that develop at floe edges may be weakened in the presence of a fully turbulent ocean, or in the presence of high sea ice or ocean velocities. In future work, it will be important to constrain the relative significance of these other physical processes and their relationship to floe size in more realistic settings. The spacing between floes is also an important length scale that influences eddy development and heat exchange, and in reality also varies in time as the floes move. Future work will need to understand the importance of this separation length scale and in particular its relationship to the ocean deformation radius, as well as the role of temporal changes in this separation length scale.

The potential combined influence of the FSTD and ocean eddies on the evolution of the sea ice cover suggests that their role in climate evolution is potentially larger than previously thought. To consider parameterizing this effect for climate studies, this mechanism must be further studied through less idealized numerical experiments, with a more detailed scaling analysis of the relationships between the length scales discussed here. Observations are needed in order to validate these results, as well as the recent predictive models of the FSD [*Zhang et al.*, 2015] and FSTD [*Horvat and Tziperman*, 2015]. The difficulty of observing the polar ocean and sea ice on the required small length and time scales remains a significant challenge in this context.

Acknowledgments. We thank Mike Spall and three anonymous reviewers for most constructive comments. We also thank Mary-Louise Timmermans for valuable comments and for pointing out an error in our preliminary model setup. This research was supported by NASA grant NNX14AH39G and by the NSF Physical Oceanography program, grant number OCE-1535800. CH was supported by the Department of Defense (DoD) through the National Defense Science & Engineering Graduate Fellowship (NDSEG) Program. ET thanks the Weizmann Institute of Science for its hospitality during parts of this work. Files required to reproduce experiments shown here are publicly available at http://www.seas.harvard.edu/climate/eli/Downloads/Sea-ice-floe-size-distribution/.

References

Aksenov, Y., E. E. Popova, A. Yool, A. G. Nurser, T. D. Williams, L. Bertino, and J. Bergh (2016), On the future navigability of Arctic sea routes: High-resolution projections of the Arctic Ocean and sea ice, *Mar Policy*, doi: 10.1016/j.marpol.2015.12.027.

Asplin, M. G., R. Galley, D. G. Barber, and S. Prinsenberg (2012), Fracture of summer perennial sea ice by ocean swell as a result of Arctic storms, *J. Geophys. Res. Oceans*, *117*(6), 1–12, doi:10.1029/2011JC007221.

Birnbaum, G., and C. Lüpkes (2002), A new parameterization of surface drag in the marginal sea ice zone, *Tellus A*, *54*(1), 107–123, doi:10.1034/j.1600-0870.2002.00243.x.

Boccaletti, G., R. Ferrari, and B. Fox-Kemper (2007), Mixed Layer Instabilities and Restratification, *J. Phys. Oceanogr.*, *37*(9), 2228–2250, doi:10.1175/JPO3101.1.

Carton, J. A., and B. S. Giese (2008), A Reanalysis of Ocean Climate Using Simple Ocean Data Assimilation (SODA), *Mon. Weath. Rev.*, *136*(8), 2999–3017, doi: 10.1175/2007MWR1978.1.

Deremble, B., N. Wienders, and W. K. Dewar (2013), CheapAML: A Simple, Atmospheric Boundary Layer Model for Use in Ocean-Only Model Calculations, *Mon. Weath. Rev.*, *141*(2), 809–821, doi:10.1175/MWR-D-11-00254.1.

Feltham, D. L. (2005), Granular flow in the marginal ice zone, *Philos. T. Roy. Soc. A*, *363*(1832), 1677–1700, doi: 10.1098/rsta.2005.1601.

Fox-Kemper, B., R. Ferrari, and R. Hallberg (2008), Parameterization of Mixed Layer Eddies. Part I: Theory and Diagnosis, *J. Phys. Oceanogr.*, *38*(6), 1145–1165, doi: 10.1175/2007JPO3792.1.

Gildor, H., and E. Tziperman (2003), Sea-ice switches and abrupt climate change., *Philos. Trans. R. Soc. London, Ser. A*, *361*(1810), 1935–1942; discussion 1942–1944, doi: 10.1098/rsta.2003.1244.

Herman, A. (2013), Numerical modeling of force and contact networks in fragmented sea ice, *Ann. Glaciol.*, *54*(62), 114–120, doi:10.3189/2013AoG62A055.

Hibler, W. D. (1979), A Dynamic Thermodynamic Sea Ice Model, *J. Phys. Oceanogr.*, *9*(4), 815–846, doi:10.1175/1520-0485(1979)009¡0815:ADTSIM¿2.0.CO;2.

Horvat, C., and E. Tziperman (2015), A prognostic model of the sea ice floe size and thickness distribution, *Cryosphere*, *9*, 2119–2134, doi:10.5194/tc-9-2119-2015.

Huang, R. X. (2005), Available potential energy in the world's oceans, *J. Mar. Res.*, *63*(1), 141–158, doi: 10.1357/0022240053693770.

Hunke, E. C., and W. H. Lipscomb (2008), CICE: the Los Alamos Sea Ice Model Documentation and Software User's Manual Version 4.0 LA-CC-06-012, *Tech. rep.*, Los Alamos Natl. Laboratory, Los Alamos, N.M.

Kanamitsu, M., W. Ebisuzaki, J. Woollen, S. K. Yang, J. J. Hnilo, M. Fiorino, and G. L. Potter (2002), NCEP-DOE AMIP-II reanalysis (R-2), *B Am Meterolog Soc*, *83*, 1631–1643, doi: 10.1175/BAMS-83-11-1631(2002)083¡1631:NAR¿2.3.CO;2.

Large, W. G., J. C. McWilliams, and S. C. Doney (1994), Oceanic vertical mixing: A review and a model with a nonlocal boundary layer parameterization, *Rev. Geophys.*, *32*(4), 363, doi: 10.1029/94RG01872.

Losch, M., D. Menemenlis, J. M. Campin, P. Heimbach, and C. Hill (2010), On the formulation of sea-ice models. Part 1: Effects of different solver implementations and parameterizations, *Ocean Model.*, *33*(1-2), 129–144, doi: 10.1016/j.ocemod.2009.12.008.

Marshall, J., and C. Hill (1997), Hydrostatic, quasi-hydrostatic, and nonhydrostatic ocean modeling, *J. Geophys. Res. Oceans*, *102*, 5733–5752.

Matsumura, Y., and H. Hasumi (2008), Brine-driven eddies under sea ice leads and their impact on the Arctic Ocean mixed layer, *J. Phys. Oceangr.*, *38*(1), 146–163, doi: 10.1175/2007JPO3620.1.

McDougall, T. J., D. R. Jackett, D. G. Wrigte, and R. Feistel (2003), Accurate and Computationally Efficient Algorithms for Potential Temperature and Density of Seawater, *J. Atmos. Ocean. Tech.*, *20*(5), 730–741.

McWilliams, J. C. (1985), Submesoscale, coherent vortices in the ocean, *Rev. Geophys.*, *23*(2), 165, doi: 10.1029/RG023i002p00165.

Notz, D., F. A. Haumann, H. Haak, J. H. Jungclaus, and J. Marotzke (2013), Arctic sea-ice evolution as modeled by Max Planck Institute for Meteorology's Earth system model, *J Adv Model Earth Sys*, *5*(2), 173–194, doi:10.1002/jame.20016.

Overpeck, J. T., M. Sturm, J. A. Francis, D. K. Perovich, M. C. Serreze, R. Benner, E. C. Carmack, F. S. Chapin, S. C. Gerlach, L. C. Hamilton, L. D. Hinzman, M. Holland, H. P. Huntington, J. R. Key, A. H. Lloyd, G. M. McDonald, J. McFadden, D. Noone, T. D. Prowse, P. Schlosser, and C. Vörösmarty (2005), Arctic system on trajectory to new, seasonally ice-free state, *Eos Trans. AGU*, *86*(34), 309, doi: 10.1029/2005EO340001.

Peralta-Ferriz, C., and R. A. Woodgate (2015), Seasonal and interannual variability of pan-Arctic surface mixed layer properties from 1979 to 2012 from hydrographic data, and the dominance of stratification for multiyear mixed layer depth shoaling, *Prog. Oceanogr.*, *134*, 19–53, doi: 10.1016/j.pocean.2014.12.005.

Rothrock, D. A., and A. S. Thorndike (1984), Measuring the sea ice floe size distribution, *J. Geophys. Res.*, *89*, 6477–6486, doi: 10.1029/JC089iC04p06477.

Smith, D. C. (2002), Arctic Ocean mixed-layer eddy generation under leads in sea ice, *J. Geophys. Res.*, *107*, 1–17, doi: 10.1029/2001JC000822.

Steele, M. (1992), Sea ice melting and floe geometry in a simple ice-ocean model, *J. Geophys. Res. Oceans*, *97*(C), 17,729, doi:10.1029/92JC01755.

Stone, P. H. (1966), On Non-Geostrophic Baroclinic Stability, *J. Atmos. Sci.*, *23*(4), 390–400, doi:10.1175/1520-0469(1966)023¡0390:ONGBS¿2.0.CO;2.

Stroeve, J. C., M. C. Serreze, M. M. Holland, J. E. Kay, J. Malanik, and A. P. Barrett (2012), The Arctic's rapidly shrinking sea ice cover: a research synthesis, *Clim. Change*, *110*(3-4), 1005–1027, doi:10.1007/s10584-011-0101-1.

Tandon, A., and C. Garrett (1994), Mixed Layer Restratification Due to a Horizontal Density Gradient, *J. Phys. Oceanogr.*, *24*(6), 1419–1424, doi:10.1175/1520-0485(1994)024¡1419:MLRDTA¿2.0.CO;2.

Thorndike, A. S., D. A. Rothrock, G. A. Maykut, and R. Colony (1975), The Thickness Distribution of Sea Ice, *J. Geophys. Res*, *80*(33), 4501, doi:10.1029/JC080i033p04501.

Timmermans, M.-L., and S. R. Jayne (2016), The Arctic Ocean Spices Up, *J. Phys. Oceanogr.*, *46*(4), 1277–1284, doi: 10.1175/JPO-D-16-0027.1.

Winton, M. (2000), A reformulated three-layer sea ice model, *J. Atmos. Ocean. Tech.*, *17*(4), 525–531, doi:10.1175/1520-0426(2000)017¡0525:ARTLSI¿2.0.CO;2.

Zhang, J., A. Schweiger, M. Steele, and H. Stern (2015), Sea ice floe size distribution in the marginal ice zone: Theory and numerical experiments, *J. Geophys. Res. Oceans*, *120*(5), 3484–3498, doi:10.1002/2015JC010770.

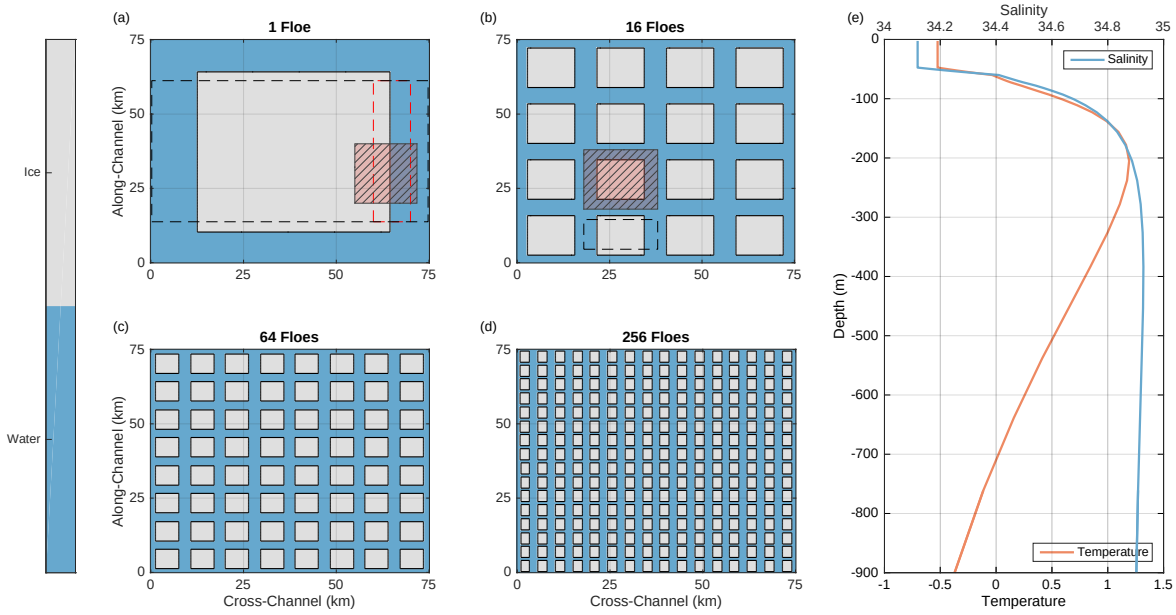

Figure 1. (a-d) Four of the seven initial sea ice "floe" configurations. Grey regions are initialized with 100% ice concentration and 1 m thickness. Blue regions have 0% ice concentration. See text for definitions of the dashed and shaded regions. (e) The initial temperature (red line, bottom axis) and salinity (blue line, top axis) profiles used in the model runs.

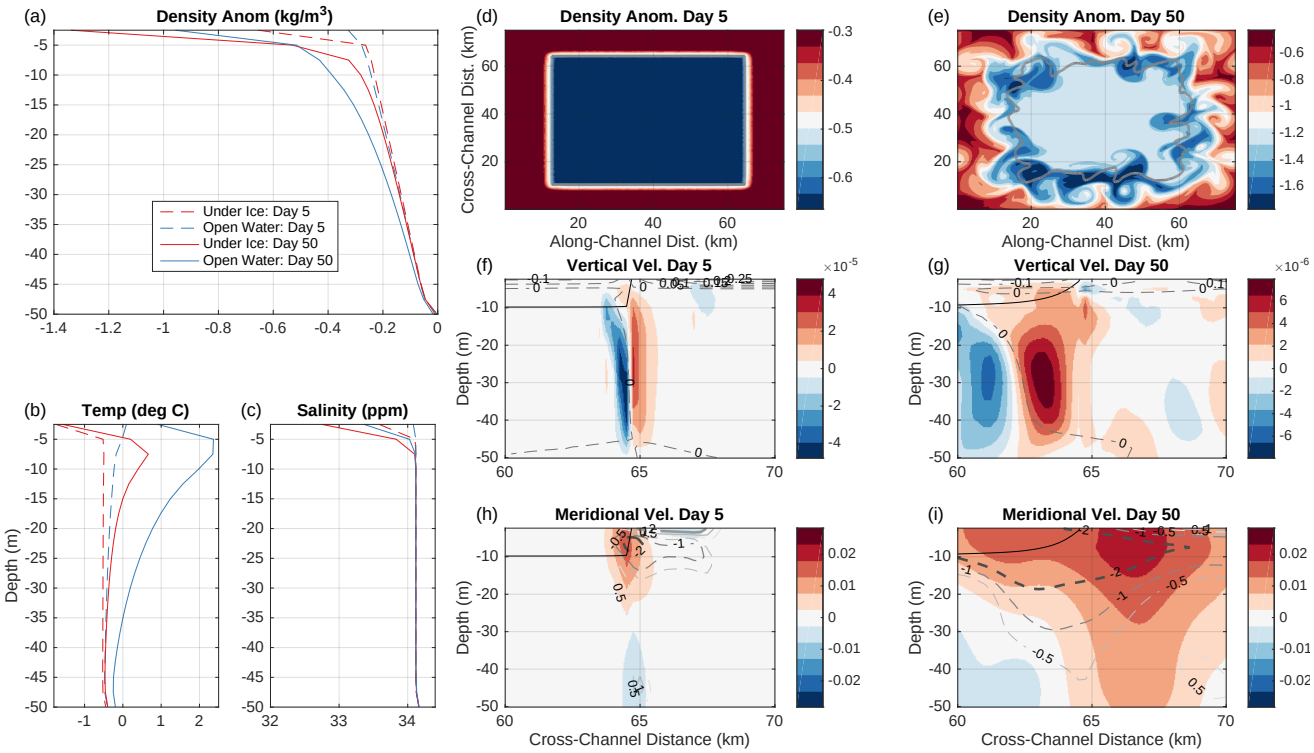

Figure 2. Circulation and stratification around and near the ice edge for a single-floe simulation (Fig. 1a). (a) Profiles of density anomaly (from the initial average surface density) at day 5 (dashed colored lines) and 50 (solid colored lines) of the simulation. Red curves are the mean density for all grid cells with at least 90% ice concentration. Blue curves are the mean density for all other points. (b) Same as (a), but for temperature. (c) same as (a), for salinity (c). (d-e) The surface density anomaly (from the initial average surface density) at days 5 and 50 of the simulation. (f-g) A depth-zonal distance section of the vertical velocity, with meridional average taken across the right-most floe edge (the region outlined in red in Fig. 1b) at days 5 and 50. (h-i) Same as (f-g), for the meridional velocity. The extent of the ice cover is indicated by black lines in (d-i), which plot the meridional average of the ice concentration across the same region, multipled by a factor of -10. Black contours in (g-h) indicate the zonal (cross-front) velocity in units of mm/s at the same times.

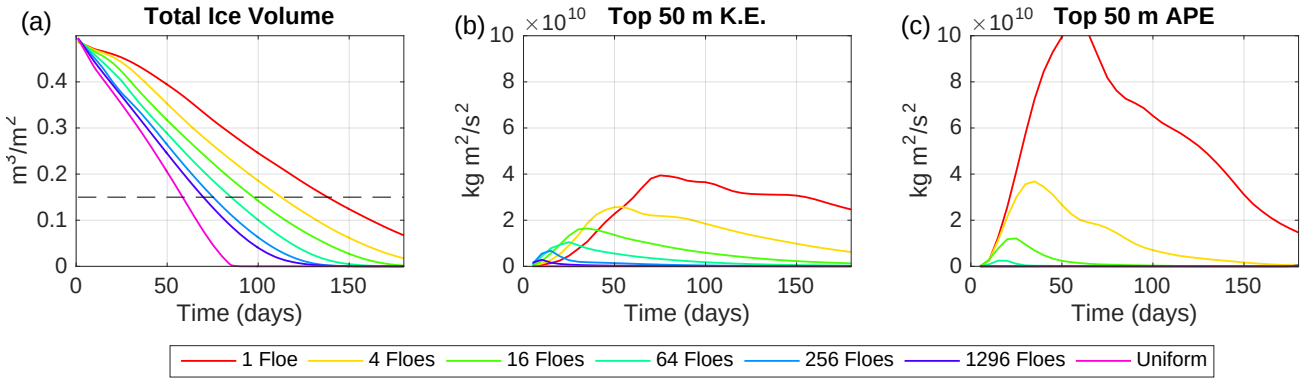

Figure 3. (a) Mean ice volume per square meter (m^3/m^2) for 1-1296 floes and for a uniform fractional ice cover run. Dashed black line indicates the point at which the mean sea ice volume decreased below 0.15 m^3/m^2. (b) Mixed layer total kinetic energy (kg m^2/s^2). (c) Mixed layer available potential energy, calculated using the method of *Huang* [2005].

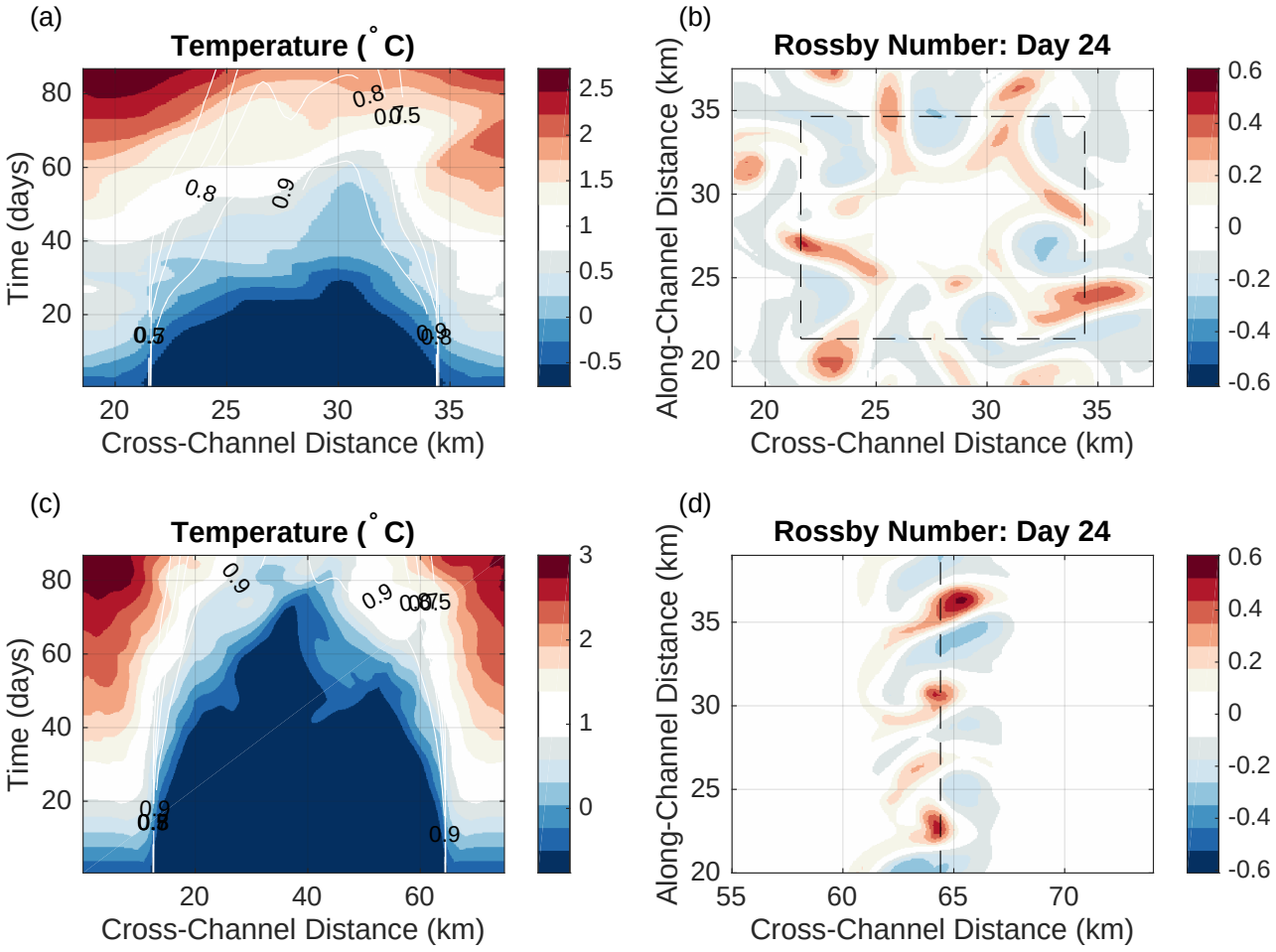

Figure 4. Spread of mixing for two different floe configurations. (a) A Hovmöller diagram of the top 10 meter mean temperature in the 16-floe experiment, where mean is taken over the meridional extent of the dashed black box shown in Fig. 1b, and the top 10 meters. Contours show the mean ice concentration over this region, with contour interval of 10%. (b) The surface Rossby number $Ro = (\frac{\partial v}{\partial x} - \frac{\partial u}{\partial y})/f$ taken over the red-grey hashed box in Fig. 1b, at day 24. (c,d) Same as (a,b), except for the case of a single floe, for similar regions shown in Fig. 1a.